

The Oxygen Non-Stoichiometry and Structure of Solid Oxide Fuel Cell Cathode Materials Measured by in-Situ Neutron Diffraction

Steven McIntosh¹, Jaap F. Vente², Wim. G. Haije² and Henny J. M. Bouwmeester³

¹Department of Chemical Engineering, University of Virginia, Charlottesville, VA 22904-4741, U.S.A. mcintosh@virginia.edu

²Energy research Centre of the Netherlands, NL-1755 ZG Petten, The Netherlands

³Inorganic Material Science, Department of Science and Technology & MESA⁺ Research Institute for Nanotechnology, University of Twente, NL-7500 AE Enschede, The Netherlands

Abstract

The mixed ion-electron conducting perovskite oxide $\text{Ba}_{0.5}\text{Sr}_{0.5}\text{Co}_{0.8}\text{Fe}_{0.2}\text{O}_{3-\delta}$ (BSCF) has recently been proposed as a promising cathode material for solid oxide fuel cells. The performance of BSCF for this application is dictated by the structure, oxygen stoichiometry, $3-\delta$, and chemical and thermal expansion properties of the material. *In-situ* neutron diffraction provides a novel approach to simultaneously measure of all of these properties at temperatures and oxygen partial pressures of interest to application; 873 to 1173 K and $p\text{O}_2$ between 5×10^{-4} to 1 atm. The related material, $\text{SrCo}_{0.8}\text{Fe}_{0.2}\text{O}_{3-\delta}$ (SCF), a promising mixed-conducting membrane material, provides an informative comparison.

It was found that BSCF exhibits significantly lower oxygen stoichiometry than SCF and that $3-\delta$ can be as low as ~ 2.2 , and ~ 2.3 respectively. This was surprising as the increased basicity of Ba^{2+} relative to Sr^{2+} may be expected to stabilize higher B-site oxidation states. In addition, where oxygen vacancies in SCF order to form the brownmillerite structure at reduced $p\text{O}_2$ and temperature, BSCF maintains the vacancy disordered cubic perovskite structure under all conditions investigated. Both of these factors will lead to increased oxygen transport rates in BSCF and may explain the observed high performance of BSCF cathodes.

Introduction

Mixed conducting perovskite structured oxides show promise as high performance cathodes for solid oxide fuel cells, SOFC. The composition $\text{Ba}_{0.5}\text{Sr}_{0.5}\text{Co}_{0.8}\text{Fe}_{0.2}\text{O}_{3-\delta}$ (BSCF) has recently been demonstrated to provide high performance as both a SOFC cathode [1] and an oxygen separation membrane [2, 3]. The parent composition $\text{SrCo}_{0.8}\text{Fe}_{0.2}\text{O}_{3-\delta}$ (SCF) has received considerable attention for application as an oxygen separation membrane due to its high ionic and electronic conductivity [4] and, consequently, high oxygen flux [5, 6]. SCF provides an interesting comparison point for discussion of BSCF.

The crystal structure and expansion properties of perovskite oxides are typically determined by high-temperature X-ray diffraction (HTXRD) and dilatometry [7, 8]. The oxygen stoichiometry is determined by either thermogravimetric analysis or coulometric titration [9-14]. In both of these methods the stoichiometry is calculated from a change in oxygen stoichiometry relative to the initial stoichiometry; determined by either reduction in hydrogen or iodometric titration. These separate measurements are then combined to evaluate the chemical expansion. In contrast, neutron diffraction allows the direct and simultaneous determination of the crystal structure, oxygen stoichiometry and relative abundance of crystal phases. This information is determined independently for each structural refinement. Here we present an *in-situ* neutron diffraction study of SCF and BSCF with the intent of emphasizing the utility of the technique in determining the structural properties of mixed-conducting oxides for application in SOFC. The experiments were carried out as a function of temperature between 873 and 1173K and oxygen partial pressure, $p\text{O}_2 = 10^{-5}$ to 1 atm. Full details of our work on SCF and BSCF are published elsewhere [15-18].

Experimental

Phase pure commercial $\text{SrCo}_{0.8}\text{Fe}_{0.2}\text{O}_{3-\square}$ (SCF) and $\text{Ba}_{0.5}\text{Sr}_{0.5}\text{Co}_{0.8}\text{Fe}_{0.2}\text{O}_{3-\square}$ (BSCF) powders (Praxair specialty ceramics, Woodinville, WA, USA) were annealed in air at 1373K for 10 hours before cooling at 0.5 K/min to room temperature. After grinding, the particle sizes (Mastersizer 2000, Malvern Instruments, Malvern, UK) were $d_{0.5} = 12.0$ and $16.5 \mu\text{m}$ and $d_{0.9} = 33.9$ and $36.6 \mu\text{m}$ for SCF and BSCF, respectively. Neutron diffraction measurements were carried out on the GEM beamline at the ISIS facility, Rutherford Appleton Laboratories, Chilton, UK. Data was collected on banks 3, 4, 5 and 6 of the GEM detector array, with d-spacing ranges of 0.5 – 1.85, 0.54 – 2.705, 0.74 – 4.1 and 1.3 – 7.15 Å respectively. ~1.5g of the sample powder was placed in a quartz sample holder with temperature measured with two thermocouples placed close to the sample but above the incoming neutron beam [16]. 50 ml/min STP of calibrated gas, oxygen in nitrogen to provide $p\text{O}_2 = 10^{-5}$ to 1 atm in decades of $p\text{O}_2$, was supplied through a quartz capillary arranged such that the gas passed through the powder sample, causing the powder to fluidize. This ensured good mixing and decreased equilibration times [16]. Diffraction patterns were collected while continually flushing the sample with the calibrated gas and monitoring the outlet $p\text{O}_2$ (Nernstian sensor, Systech Instruments, Oxford, UK).

The samples were allowed to equilibrate, determined as no change in lattice parameter, at 600°C before measurement during temperature ramps, 1.33 K/min. The measurement time for each diffraction pattern was dependent on the intensity of the incoming beam and resulted in a temperature spread between 5 and 10K for each pattern. Rapid equilibration of the samples during the heating ramp was confirmed by repeated measurements from different starting points [15, 16]. Structural information and oxygen stoichiometries were extracted from Rietveld refinement [19] using the GSAS suite of programs [20]. The combined quality of fit parameter, χ^2 , was less than two for all of the

data presented here. A detailed discussion of these measurements is presented elsewhere [15, 16].

Results and Discussion

BSCF has the cubic perovskite structure, space group $Pm\bar{3}m$, over the entire temperature and pO_2 range investigated. This structure is indicative of fully disordered vacancies on the oxygen sublattice. Figure 1a shows the lattice parameter of BSCF as a function of temperature and pO_2 . There are two components to the observed changes in lattice parameter; classical thermal expansion and chemical expansion induced by reduction of the B-site cations with increasing temperature and decreasing pO_2 . The lattice expands as the B-site cation radius increases with decreasing charge. This decrease in B-site charge is accompanied by the formation of oxygen vacancies, δ , through charge compensation. This chemical expansion leads to the observed increase in lattice parameter with decreasing pO_2 .

In contrast to this, SCF exhibits oxygen vacancy ordering at reduced T and pO_2 . For reasons of clarity, only the lattice parameters for the pure cubic perovskite phase are shown in Figure 3. At a pO_2 of 1 atm, the cubic perovskite phase is stable over the whole temperature range; however, an oxygen vacancy ordered brownmillerite phase, $Sr_2Co_{1.6}Fe_{0.8}O_5$ with space group $Icmm$, was observed below 1021K and 1020K at pO_2 of 10^{-2} and 5×10^{-4} atm, respectively. The transition between the two phases occurs through a two-phase region denoted in Figure 1. The edges of the two-phase regions were determined as the point at which two-phase refinement led to poorer quality of fit when compared to single phase refinements. As with BSCF, chemical expansion of the cubic perovskite phase leads to increasing lattice parameter with decreasing pO_2 .

It should be noted that the lattice parameter of the cubic BSCF phase is significantly larger than the equivalent SCF phase across the T- pO_2 range investigated. At 1073K and a pO_2 of 1 atm, the lattice parameters are 4.041647(3) Å and 3.93852(3) Å for BSCF and SCF respectively.

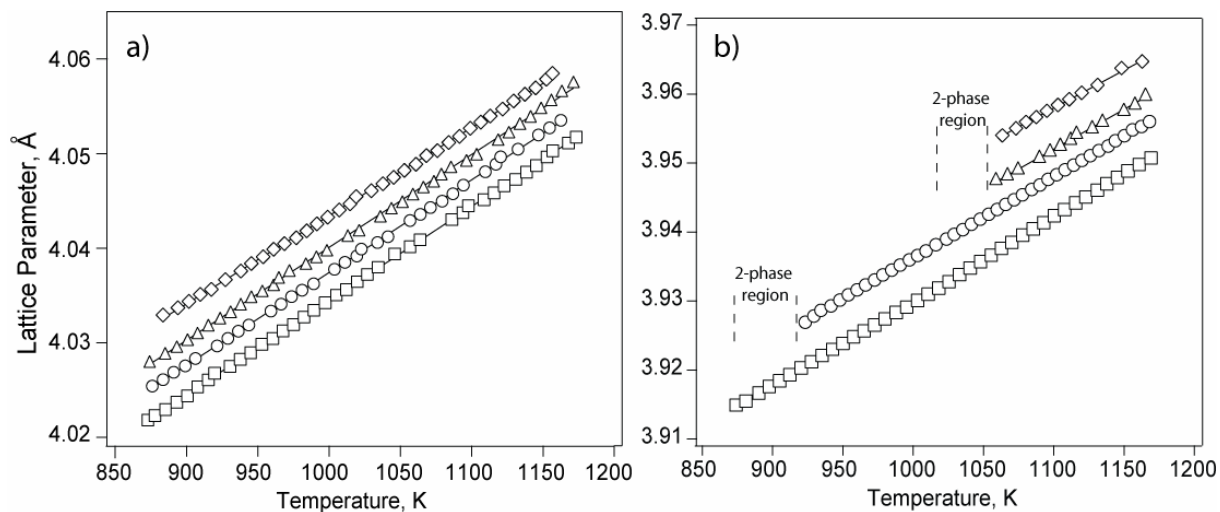


Figure 1: Lattice parameter vs. temperature of the cubic perovskite phase of a) $Ba_{0.5}Sr_{0.5}Co_{0.8}Fe_{0.2}O_{3-d}$ and b) $SrCo_{0.8}Fe_{0.2}O_{3-d}$ determined by neutron diffraction at $pO_2 = 1$ (\square), 10^{-1} (\circ), 10^{-2} (\triangle) and 10^{-3} (\diamond) atm for BSCF and 5×10^{-4} (\diamond) atm for SCF.

Figure 2 shows the oxygen stoichiometry of BSCF and SCF determined from the structural refinements. The oxygen stoichiometry of the brownmillerite phase was fixed at the ideal stoichiometry of 2.5 relative to the perovskite composition $\text{SrCo}_{0.8}\text{Fe}_{0.2}\text{O}_{3-\delta}$. Refining the stoichiometry introduced scatter within one standard deviation of the ideal stoichiometry and did not improve the quality of fit. The oxygen stoichiometry of BSCF is in good agreement with that determined by thermogravimetric measurements [16], confirming the accuracy of the technique

Our initial hypothesis was that the increased basicity of Ba^{2+} in comparison to Sr^{2+} would stabilize the higher oxidation states of the B-site cations, leading to increased oxygen stoichiometry of BSCF in comparison to SCF. However, the oxygen stoichiometry of BSCF is significantly lower than SCF over the entire $p\text{O}_2$ -T range probed; that is, doping with Ba^{2+} stabilizes the lower oxidation states of the B-site cations. Indeed, the low oxygen stoichiometry of BSCF suggests that we may be close to the stability limit for this material at 1173K and a $p\text{O}_2$ of 10^{-4} atm. One explanation for this is the larger size of Ba^{2+} when compared to Sr^{2+} . This leads to the increased lattice parameter for BSCF and is congruent with an increased average A-O and B-O bond distance in BSCF. At 1073K in air, the A-O and B-O bond distances 2.02082(2) Å and 1.96926(1) Å for BSCF and SCF respectively. The increase in bond distance will lead to decreased electron density around the B-site cations and, therefore, destabilize the higher oxidation states relative to SCF. However, it should be noted that the lattice parameter for BSCF is influenced by both the larger size of the Ba^{2+} cation and the lower oxygen stoichiometry through chemical expansion.

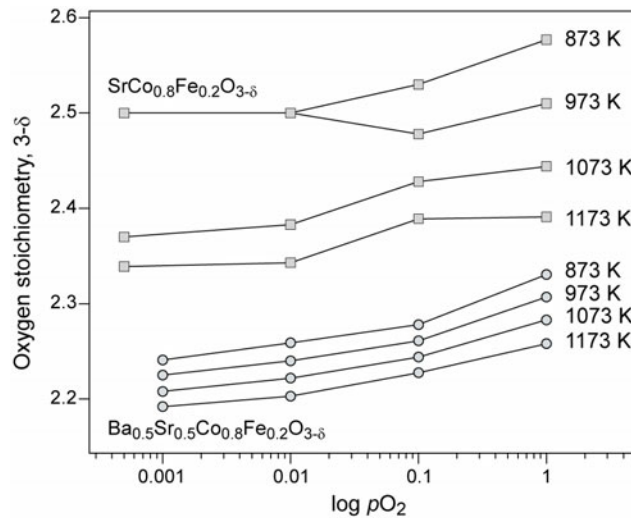


Figure 2: Oxygen stoichiometry vs. $p\text{O}_2$ of $\text{Ba}_{0.5}\text{Sr}_{0.5}\text{Co}_{0.8}\text{Fe}_{0.2}\text{O}_{3-\delta}$ (○) and $\text{SrCo}_{0.8}\text{Fe}_{0.2}\text{O}_{3-\delta}$ (□) determined by neutron diffraction.

Combining the data for cubic perovskite lattice parameter and oxygen stoichiometry allows calculation of the total, thermal and chemical expansion coefficients of BSCF and SCF [15, 16]. The chemical strain is defined as

$$\varepsilon_c = \left. \frac{(a - a_0)}{a_0} \right|_{T=\text{constant}}$$

Where a is the lattice parameter and a_0 is the lattice parameter at a reference state. The chemical expansion coefficient is then defined as $\epsilon_c/\Delta\delta$ where $\Delta\delta$ is the change in oxygen stoichiometry leading to the strain. The chemical expansion of BSCF and SCF at 1073K were 0.019(2) and 0.05(1) $\times 10^{-6}$ respectively.

In addition to analysis of the cubic perovskite phase, neutron diffraction allows a detailed analysis of the brownmillerite phase and the phase transition in SCF. Figure 3 shows the 50% probability thermal ellipsoid representation of the ideal brownmillerite structure, space group $Ibm2$. This ideal brownmillerite structure is shown for clarity. The refined space group for SCF brownmillerite is $Icmm$ which differs from $Ibm2$ by splitting the Co/Fe(2) and O(3) sites. This allows two possible orientations of each tetrahedron, with a 50% probability of either orientation, and represents incomplete ordering of the brownmillerite phase. The size and orientation of the ellipsoids in Figure 3 are taken from the neutron diffraction refinements for the $Icmm$ space group.

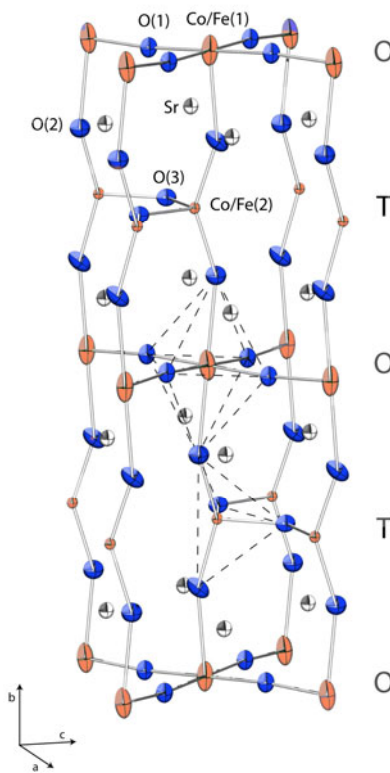


Figure 3: 50% probability thermal ellipsoidal representation of the brownmillerite phase of $\text{SrCo}_{0.8}\text{Fe}_{0.2}\text{O}_{3-\delta}$ at 923 K, $p\text{O}_2 = 5 \times 10^{-4}$ atm. For reasons of clarity, the $Ibm2$ space group is depicted instead of the $Icmm$ structure refined from neutron diffraction.

A subset of the full structural information available from neutron diffraction measurements is shown in Figure 4. The data shown is for SCF at a $p\text{O}_2$ of 10^{-2} atm between 873 and 1173 K. Figure 4a shows the lattice parameters of the brownmillerite and cubic perovskite phases. The lattice parameters of the brownmillerite phase are scaled to $a/\sqrt{2}$, $b/4$, and $c/\sqrt{2}$ to aid comparison with the cubic unit cell. As the temperature is increased from 873 K, the brownmillerite lattice expands until the start of the two phase region at 1020 K where the lattice starts to contract. At the upper temperature edge of the two phase region, the brownmillerite lattice parameters show an abrupt shift towards the cubic cell value. This sudden change in brownmillerite lattice parameter is associated with the final fraction of the brownmillerite phase transforming into the cubic perovskite, as

shown in Figure 4b. The cell volume of the brownmillerite phase is significantly larger than that of the coexisting cubic phase in this two-phase region, 1.265(2) % at 1021 K. Such a change in lattice volume may complicate application of this material. At higher temperatures, only the cubic phase is present.

The oxygen stoichiometry of SCF decreases abruptly as the vacancy ordered brownmillerite phase transforms into the vacancy disordered cubic perovskite, as shown in Figure 4c. A smoother transition from the brownmillerite phase to a pure cubic perovskite structure with refined oxygen stoichiometry of 2.50(2) was observed at 869 K and $pO_2 = 10^{-1}$ atm[15], further confirming the accuracy of the technique. The cubic perovskite stoichiometry decreases smoothly as the temperature is increased. Finally, figure 4d shows the Co/Fe-O bond distances within the Co/Fe octahedra. The equatorial Co/Fe(1)-O(1) bond length in the brownmillerite phase is comparable to the Co/Fe-O bond distance in the cubic perovskite and shows a relatively smooth transition through the two-phase region. In contrast to this, the apical Co/Fe(1)-O(2) bond is significantly larger than in the cubic perovskite phase representing a significant distortion of the octahedral layer. This distance decreases rapidly through the two-phase region as the brownmillerite phase transforms to the cubic perovskite.

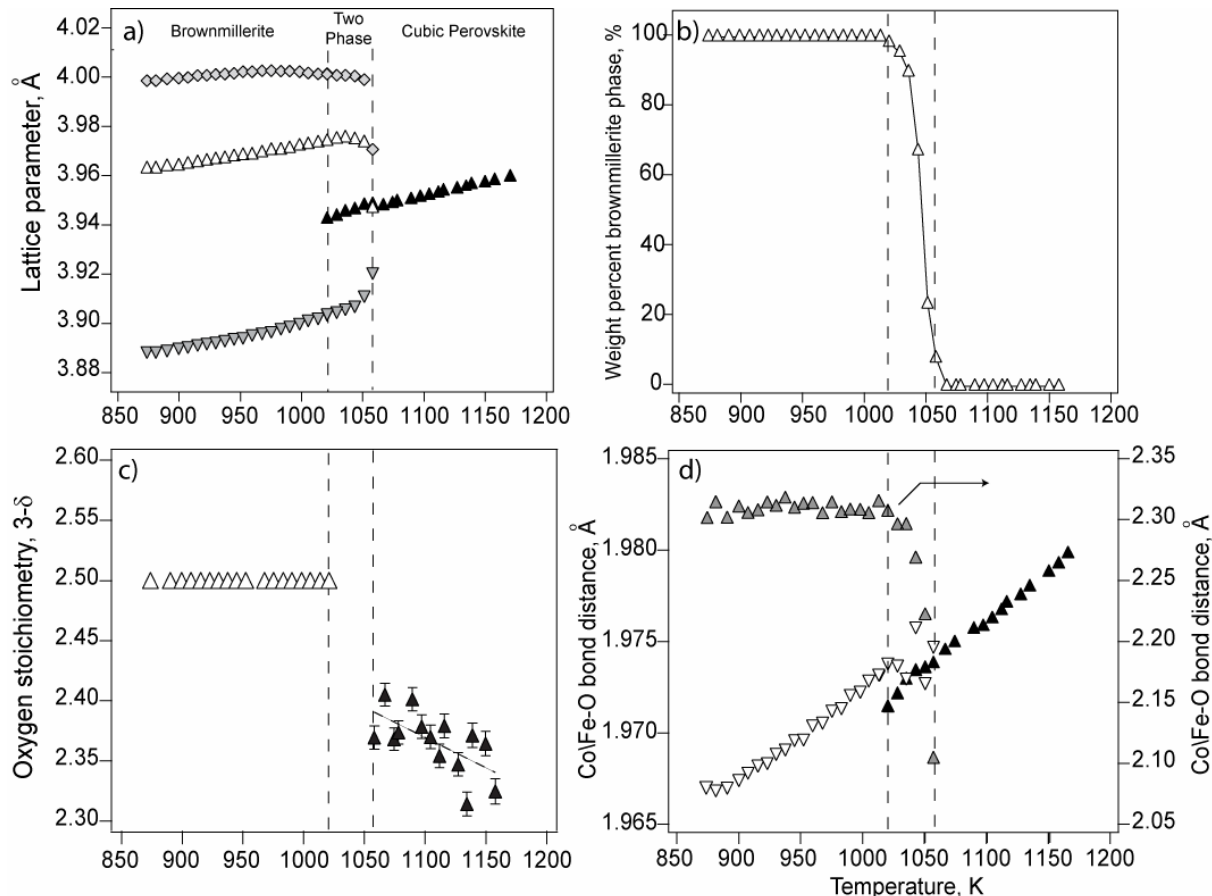


Figure 4: SrCo_{0.8}Fe_{0.2}O_{3-x} a) lattice parameters $a/\sqrt{2}$ (Δ), $b/4$ (\diamond), and $c/\sqrt{2}$ (∇) for the brownmillerite phase and a (\blacktriangle) for the cubic perovskite, b) percentage brownmillerite phase vs. temperature, c) oxygen stoichiometry of the brownmillerite and cubic perovskite phase and d) equatorial Co/Fe(1)-O(1) (∇) and apical Co/Fe(1)-O(2) (\blacktriangle), bond distances in the brownmillerite, and Co/Fe-O bond distance in the cubic perovskite (\blacktriangle) phase versus temperature at $pO_2 = 10^{-2}$ atm.

Conclusions

In-situ neutron diffraction is a powerful technique that yields a wide range of information of relevance to SOFC materials development. This includes the lattice parameters, bond distances and relative abundance of co-existing phases. Perhaps of most significance is the simultaneous determination of these crystallographic parameters and the oxygen stoichiometry. Unlike traditional techniques, the oxygen stoichiometry is determined independently for each diffraction pattern.

Regarding the materials investigated in this study, the high performance of BSCF cathodes may be related to the high concentration of oxygen vacancies within the cubic perovskite lattice of BSCF relative to other materials. This increased vacancy concentration is preliminarily attributed to the increased size of Ba^{2+} relative to Sr^{2+} . The phase transition of the vacancy ordered brownmillerite to the cubic perovskite phase of SCF is associated with decrease in oxygen stoichiometry and a contraction of the distorted apical Co/Fe(1)–O(2) bond.

References

1. Z.P. Shao and S.M. Haile, *Nature* **431** (2004) (7005), p. 170.
2. Z. Shao, G. Xiong, J. Tong, H. Dong and W. Yang, *Separation and Purification Technology* **25** (2001) (1-3), p. 419.
3. Z. Shao, W. Yang, Y. Cong, H. Dong, J. Tong and G. Xiong, *J. Membr. Sci.* **172** (2000) (1-2), p. 177.
4. Y. Teraoka, H.M. Zhang, K. Okamoto and N. Yamazoe, *Mater. Res. Bull.* **23** (1988) (1), p. 51.
5. H. Kruidhof, H.J.M. Bouwmeester, R.H.E. Doorn and A.J. Burggraaf, *Solid State Ionics* **63-65** (1993), p. 816.
6. L. Qiu, T.H. Lee, L.M. Liu, Y.L. Yang and A.J. Jacobson, *Solid State Ionics* **76** (1995) (3-4), p. 321.
7. A. Atkinson and T.M.G.M. Ramos, *Solid State Ionics* **129** (2000) (1-4), p. 259.
8. X.Y. Chen, J.S. Yu and S.B. Adler, *Chem. Mater.* **17** (2005) (17), p. 4537.
9. M.H.R. Lankhorst and H.J.M. Bouwmeester, *J. Electrochem. Soc.* **144** (1997) (4), p. 1261.
10. M.H.R. Lankhorst and H.J.M. Bouwmeester, *J. Electrochem. Soc.* **144** (1997) (4), p. 1268.
11. J. Mizusaki, Y. Mima, S. Yamauchi, K. Fueki and H. Tagawa, *J. Solid State Chem.* **80** (1989) (1), p. 102.
12. J. Mizusaki, M. Yoshihiro, S. Yamauchi and K. Fueki, *J. Solid State Chem.* **58** (1985) (2), p. 257.
13. M.H.R. Lankhorst, H.J.M. Bouwmeester and H. Verweij, *J. Solid State Chem.* **133** (1997) (2), p. 555.
14. L.M. Liu, T.H. Lee, L. Qiu, Y.L. Yang and A.J. Jacobson, *Mater. Res. Bull.* **31** (1996) (1), p. 29.
15. S. McIntosh, J.F. Vente, W.G. Haije, D.H.A. Blank and H.J.M. Bouwmeester, *Solid State Ionics* **177**, (2006), p. 833.
16. S. McIntosh, J.F. Vente, W.G. Haije, D.H.A. Blank and H.J.M. Bouwmeester, *Chem. Mater.* **18** (2006) (8), p. 2187.
17. S. McIntosh, J.F. Vente, W.G. Haije, D.H.A. Blank and H.J.M. Bouwmeester, *Solid State Ionics In Press* (2006)
18. J.F. Vente, S. McIntosh, W.G. Haije and H.J.M. Bouwmeester, *Journal of Solid State Electrochemistry* **10** (2006), p.581.
19. H.M. Rietveld, *J. Appl. Crystallogr.* **2** (1969), p. 65.
20. A.C. Larson and R.B. Von Dreele, *Los Alamos National Laboratory Report LAUR* (2000), p. 86.